CrossMark
click for updates

Impact of carbon nanotube length on electron transport in aligned carbon nanotube networks

Jeonyoon Lee,[1,a)] Itai Y. Stein,[1,a)] Mackenzie E. Devoe,[2] Diana J. Lewis,[3] Noa Lachman,[3] Seth S. Kessler,[4] Samuel T. Buschhorn,[3] and Brian L. Wardle[3,b)]

[1]*Department of Mechanical Engineering, Massachusetts Institute of Technology, 77 Massachusetts Ave., Cambridge, Massachusetts 02139, USA*
[2]*Department of Materials Science and Engineering, Massachusetts Institute of Technology, 77 Massachusetts Ave., Cambridge, Massachusetts 02139, USA*
[3]*Department of Aeronautics and Astronautics, Massachusetts Institute of Technology, 77 Massachusetts Ave., Cambridge, Massachusetts 02139, USA*
[4]*Metis Design Corporation, 205 Portland St., Boston, Massachusetts 02114, USA*

Here, we quantify the electron transport properties of aligned carbon nanotube (CNT) networks as a function of the CNT length, where the electrical conductivities may be tuned by up to $10\times$ with anisotropies exceeding 40%. Testing at elevated temperatures demonstrates that the aligned CNT networks have a negative temperature coefficient of resistance, and application of the fluctuation induced tunneling model leads to an activation energy of $\approx 14\,\mathrm{meV}$ for electron tunneling at the CNT-CNT junctions. Since the tunneling activation energy is shown to be independent of both CNT length and orientation, the variation in electron transport is attributed to the number of CNT-CNT junctions an electron must tunnel through during its percolated path, which is proportional to the morphology of the aligned CNT network. © 2015 AIP Publishing LLC.
[http://dx.doi.org/10.1063/1.4907608]

The quantum confinement mediated landmark properties of one dimensional materials, such as nanowires, nanofibers, and nanotubes, makes them attractive to a number of high value applications. Recently, carbon nanotubes (CNTs) were extensively studied in scalable aligned architectures, commonly known as forests, which promise the design and facile manufacture of multifunctional material architectures with tunable properties.[1,2] When the aligned CNTs (A-CNTs) are densified using a rigid roller, a network comprising CNTs aligned in a desired direction can be synthesized, forming a CNT film similar to buckypaper. Recent studies indicate that A-CNT networks can find many uses including sensors and actuators,[3–7] optoelectronics,[5–11] and energy storage architectures.[7,12–14] However, the dependence of the electron transport properties of A-CNT networks on the length of the underlying CNTs in such complex systems is still poorly understood. In this letter, we evaluate the impact of CNT length on the electron transport properties of A-CNT networks and demonstrate that the CNT morphology is responsible for the scaling behavior of the sheet resistance as a function of CNT length at different temperatures.

While the intrinsic electrical properties of single and multiwalled CNTs were extensively studied both experimentally and theoretically,[1,2,5] most previous studies on the electrical properties of CNT networks focus on single walled CNT architectures formed using solution processing.[15–21] Since these networks are normally thin and comprised of single walled CNTs that are $\lesssim 50\,\mu m$ long,[15–21] our understanding of the impact of morphology on electron transport in thick CNT networks comprised of long ($\gtrsim 100\,\mu m$)

multiwalled CNTs remains incomplete. Recent work on A-CNT networks made via roller densification of $\gtrsim 100\,\mu m$ long vertically aligned CNT arrays showed that the sheet resistance is directly proportional to the density of the network[22] and is mildly anisotropic in nature.[23,24] However, an important factor that was largely absent from these studies was CNT length. Previous studies indicated that A-CNT arrays comprised of longer CNTs have significantly higher resistances,[24] but since these reports do not describe and model the electron transport mechanism, further work is necessary to elucidate the importance of CNT length on the electronic properties of A-CNT networks made via densification of A-CNT arrays. Here, we use a four probe method to quantify the impact of CNT length on the anisotropic sheet resistance and include bonding character information from Raman spectroscopy to study the underlying physics that govern electron transport in such networks.

A-CNT arrays were grown in a 44 mm internal diameter quartz tube furnace at atmospheric pressure via a thermal catalytic chemical vapor deposition process, very similar to a previously described process,[25–27] with ethylene as the carbon source and 600 ppm of water vapor added to the inert gas. The CNTs were grown on $3\,\mathrm{cm} \times 4\,\mathrm{cm}$ Si substrates forming A-CNT arrays that are up to $\approx 300\,\mu m$ tall and are composed of multiwalled CNTs that have an average outer diameter of $\approx 7.8\,\mathrm{nm}$ (3–7 walls[28] with an average inner diameter of $\approx 5.1\,\mathrm{nm}$), evaluated intrinsic CNT density of $\approx 1.6\,\mathrm{g/cm}^3$,[29] average inter-CNT spacing of $\approx 59\,\mathrm{nm}$, and corresponding volume fraction of $\approx 1.6\%$ CNTs.[27] See Sec. S1 in the supplementary material[30] for further details. The height of the as-grown A-CNT arrays, defined as H, was evaluated by measuring the stage displacement necessary for an optical microscope (Carl Zeiss Axiotech 30 HD) to

a)J. Lee and I. Y. Stein contributed equally to this work.
b)Electronic mail: wardle@mit.edu

transition from focusing onto the Si wafer (the bottom of the CNT forest) to the top of the CNT forest. The true length of the CNTs (L) can be approximated by correcting the H values for the CNT waviness (waviness ratio ~ 0.25 for these as-grown A-CNTs),[31] and the $\lesssim 0.1-1 \mu m$ thick growth initiation region,[32] which leads to an approximation of $L \sim 1.5 H$ here (see Sec. S2 in supplementary material[30] for details). The A-CNTs were re-oriented and densified using a 10 mm diameter rod and Guaranteed Nonporous Teflon (GNPT) film by rolling in the desired alignment directions (see Fig. 1 for illustration). Since the post-growth H_2 anneal step weakens the attachment of the CNTs to the catalyst layer,[33] the A-CNT network adheres to the GNPT film and is cleanly removed from the Si substrate. See Fig. 1 for high resolution scanning electron microscopy (JEOL 6700, 3.0 mm working distance) micrographs of the cross sectional morphology of an as-grown A-CNT array (1.0 kV accelerating voltage), and an A-CNT network produced via the densification of an A-CNT array (1.5 kV accelerating voltage).

While the electrical conductivity is the most common measure used to quantify the electrical properties of CNT networks regardless of their alignment, sheet resistance is a more representative measure of the electron transport in the A-CNT networks studied here. This originates from the uncertainty in the L values approximated from the experimentally determined H ($\rightarrow L \sim 1.5 H$ here), which prevents the CNT networks from being treated as bulk materials without potentially inducing large errors in the measured electrical properties. Because contact resistance could play a role on the sheet resistance of the A-CNT networks, the sheet resistance was evaluated using a four-point probe method (Keithley SCS-4200)[34] where electrode-CNT connections were established using Ag paint. Since defects present in the CNTs can lead to vastly altered electronic properties,[35–38] the defect concentration of the CNTs that comprise the networks was quantified via Raman spectroscopy. Raman spectra were collected using a Raman microscope (LabRam HR800, Horiba Jobin Yvon) with 532 nm (2.33 eV) laser excitation through a $50\times$ objective (N.A. 0.75), and defect concentrations were evaluated using the integrated intensities

(area ratios) of the G ($\sim 1350 \mathrm{cm}^{-1}$) and D ($\sim 1580 \mathrm{cm}^{-1}$) peaks,[39] known as the A_G/A_D ratio.[40] Additionally, since the electronic properties strongly depend on the CNT-CNT junction potentials, which are a strong function of temperature, the thermal response of electron transport was quantified by evaluating the scaling of the sheet resistance of the A-CNT networks from 25 °C to 130 °C (via a hot plate).

As illustrated by Fig. 2(a), the Raman spectra of the CNTs do not vary significantly as a function of L. The resulting values of the A_G/A_D ratios, which were all $\approx 0.7 \pm 0.1$, confirm that the wall defect concentrations are of similar magnitude, meaning that the intrinsic properties of the CNTs are invariant with L in this study. To test the impact of L on the electrical transport properties of the A-CNT networks, the sheet resistance (R) was measured and is presented as a function of L in Fig. 2(b). As Fig. 2(b) demonstrates, the R values show a very strong dependence on L, starting at ≈ 75 $\Omega/\square$ for $L \approx 90 \mu m$, and decreasing to ≈ 10 $\Omega/\square$ for $L \approx 465 \mu m$. These resistance values are lower than most of the ones previously reported for graphene and CNT film based microheaters.[41] Using a film thickness of $\sim 10 \mu m$

FIG. 2. (a) Raman spectra illustrating that the bond character does not vary significantly as a function of the CNT length (L). (b) Sheet resistance (R) as a function of L indicating that the electron transport in the A-CNT networks strongly depends on the length of the CNTs that comprise them. Inset: R of A-CNT networks as a function of orientation θ, a ratio of $R(\theta = 90°)/R(\theta = 0°) \sim 1.4$ was observed.
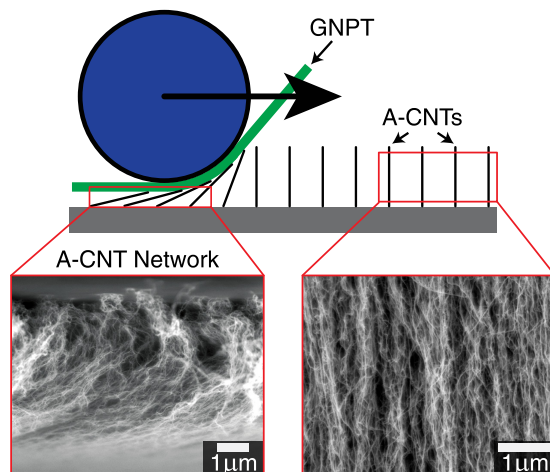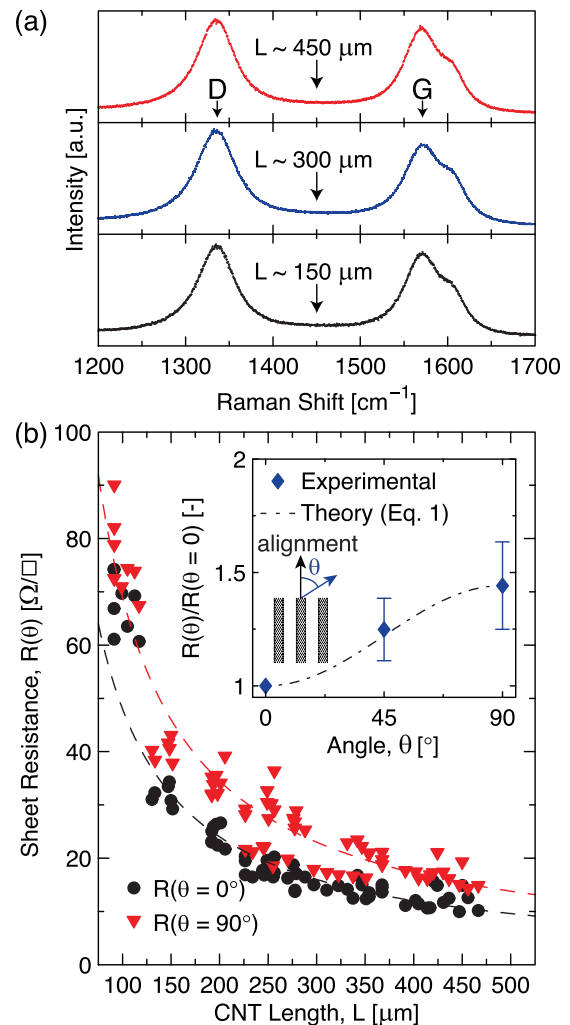

FIG. 1. Illustration of the densification process (top), and cross-sectional morphology of an A-CNT array (bottom right) and the networks produced from their densification via rolling (bottom left).

yields order of magnitude electrical conductivities of ~ 10 S/cm for $L \approx 90\,\mu m$ and ~ 100 S/cm for $L \approx 465\,\mu m$, in good agreement with the previous work on A-CNT networks and related architectures.[23,24,42] Since the intrinsic CNT properties are invariant with L (based on the Raman spectra), the large changes in R can be attributed to the impact of the A-CNT network morphology on the number and quality of electron pathways available for electron transport. Previous work on percolated CNT networks showed that $R \propto cL^{-n}$ where c and n are constants. A study on single walled CNTs with $L \lesssim 4\,\mu m$ showed that $n \approx 1.46$, and that the power law relationship holds until the resistance along the CNT (i.e., the intrinsic resistance of the CNT, which scales linearly with L)[43] becomes comparable to the CNT-CNT junction resistance ($L \gtrsim 25\,\mu m$ in the previous work).[15] This value of n is within the expected range of values for a percolated network of conductive fibers, where n was previously shown to range from a lower bound of $n = 0$ (junction resistance is negligible $\rightarrow R$ independent of L) to an upper bound of $n = -2.48$ (junctions completely dominate R).[15,44] Application of this model yields a $R \propto cL^{-1}$ dependence (see Fig. 2(b)), meaning that CNT-CNT coupling is what limits the electron transport properties in the A-CNT networks and not the intrinsic CNT resistance. These results indicate that the previously proposed scaling relationship is appropriate for A-CNT networks with CNTs that are more than an order of magnitude longer than those of Hecht *et al.*[15] and are consistent with previous work that reported and/or assumed that the CNT intrinsic resistance is much smaller than that of the CNT-CNT junction resistance.[15,16] Since the intrinsic properties of CNTs are highly anisotropic, the importance of morphology was further studied by evaluating R as a function of the orientation angle, θ (see Fig. 2(b) inset), as follows:

$$R(\theta) = R(\theta = 0^\circ)\cos^2(\theta) + R(\theta = 90^\circ)\sin^2(\theta). \quad (1)$$

See Sec. S3 in supplementary material[30] for the derivation of Eq. (1) from matrix transformations. As illustrated by the inset of Fig. 2(b), $R(\theta)$ for $L > 150\,\mu m$ showed anisotropy on the order of $\sim 40\%$ ($R(\theta = 90^\circ)/R(\theta = 0^\circ) \approx 1.44 \pm 0.19$), and the experimentally determined $R(\theta = 45^\circ)$ values showed good agreement with the predictions of Eq. (1) (using $R(\theta = 90^\circ)/R(\theta = 0^\circ) \sim 1.44$). $R(\theta)$ for $L < 150\,\mu m$ exhibited much lower anisotropy ($R(\theta = 90^\circ)/R(\theta = 0^\circ) \approx 1.19 \pm 0.13$) due to squashing and/or buckling during the densification process (see Fig. S5 in supplementary material[30]) and is therefore not included in the inset of Fig. 2(b) due to the altered morphology. Further work is necessary to determine the degree of buckling/squashing (i.e., excess waviness that leads to additional potential CNT-CNT junctions in the in-plane directions, misalignment of the CNTs, etc.) that occurs during the densification of A-CNT arrays with $L < 150\,\mu m$ via a rigid roller. Since the CNT-CNT junction potentials are a strong function of temperature, the physics that underlie electron transport in the A-CNT networks was further studied by evaluating the temperature response of R.

Since the electrical conductivity of thick CNT networks is limited by the CNT-CNT junction resistance (see Fig. 3(a) for the conduction mechanism),[45–49] their temperature coefficient of resistance (TCR) is expected to have a negative value (i.e., nonmetallic behavior).[46] As Fig. 3(b) demonstrates, the TCR for the A-CNT networks used in this study is $\approx -1.2 \times 10^{-3}$ K^{-1}, which is consistent with those reported in the previous studies (-0.4 to -1.4×10^{-3} K^{-1}).[23,24,50] Since the activation energy (E_a) for electron transport via tunneling in the CNT-CNT junction decreases with the number of walls of the CNTs in the network,[50] the order of magnitude span of the TCR in the previous work can be attributed to the differences in CNTs that comprised the networks. Another factor that could account for the TCR range in the literature is a difference in the CNT curvature and inter-CNT spacing distribution, which leads to lower junction resistances for preferentially aligned CNTs with large contact areas. Since these CNT networks are relatively thick and have native inter-layer bonds that likely enable electrons to navigate around defects in the outer walls, their electron transport mechanism will be better represented using the fluctuation induced tunneling conduction (FITC) model,[46–48] as opposed to the 1D, 2D, and 3D variable range hopping (VRH) model that many previous studies have adopted to analyze the thermal response of the electrical properties of thin single walled CNT networks.[51,52] To evaluate E_a using the FITC model, the following expression can be applied:[53–55]

$$\frac{R(T)}{R(T_o)} = \beta \exp\left(\frac{T_b}{T + T_s}\right), \quad (2)$$
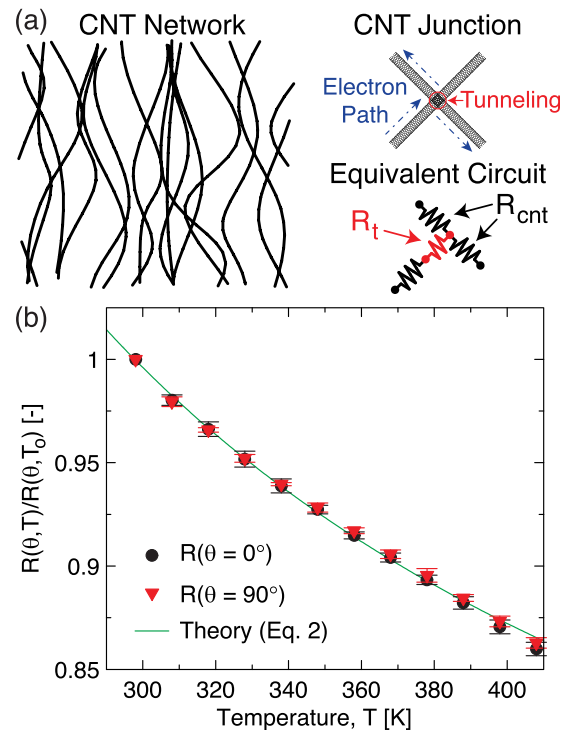

FIG. 3. (a) Illustration of the FITC mechanism which dominates the thermal response of the electron transport properties in the A-CNT networks. The intrinsic resistance of the CNT (R_{cnt}) and the tunneling resistance (R_t) are indicated. (b) Sheet resistance (R) as a function of the operating temperature (T). Evaluation of the parameters of Eq. (2) indicates that the activation energy for tunneling is ≈ 14.2 meV independent of orientation (θ) and CNT length.

where T_b corresponds to the tunneling activation energy, T_s defines the point at which thermal activation occurs, T_o is the reference temperature ($T_o = 298$ K here), and β is a scaling parameter. Fitting the experimental data (See Fig. 3(b)) yields the following parameters for Eq. (2) (coefficient of determination $= 0.9976$): $\beta = 0.581$, $T_b = 165$ K,   and $T_s = 6.10$ K. The value of $T_b/T_s \approx 27$ indicates that the fitting parameters are consistent with the previous investigations utilizing the FITC model.[53–55] E_a can now be evaluated using kT_b, where k is the Boltzmann constant, yielding $E_a \approx 14.2$ meV. This value is consistent with previous work on electron transport in CNT networks.[46,50] Since the fitting parameters for Eq. (2) can be applied to data from both $R(\theta = 0°)$ and $R(\theta = 90°)$ with the same coefficient of determination ($=0.9976$), these results indicate that E_a is independent of both L and θ in the A-CNT networks. Such a finding is consistent with the Raman spectroscopy results, which show that the CNT quality does not vary significantly with L, leading to a CNT-CNT junction resistance that is consistent throughout all the A-CNT networks studied here. Since the experimental data included in Fig. 3(b) originates from aligned CNT networks with a wide distribution of CNT volume fractions ($\propto$ number of junctions per CNT),[16] but the E_a is approximately constant, Fig. 3(b) indicates that higher CNT confinement has little influence on the junction resistance.

In summary, the scaling of the sheet resistance of the A-CNT networks was observed to be inversely proportional to the CNT length, and range from ≈ 80 $\Omega/\square$ for short CNTs (lengths $\lesssim 100\,\mu$m) to ≈ 10 $\Omega/\square$ for long CNTs (lengths $\gtrsim 300\,\mu$m). Also, the sheet resistance is shown to vary as a function of orientation by up to $\sim 50\%$. Since Raman spectroscopy indicates that the defect concentration in the CNTs is not a function of their length, and the thermal dependence of the sheet resistance indicates that the activation energy for electron transport via tunneling in the CNT-CNT junctions (≈ 14.2 meV) is independent of both CNT length and orientation, the scaling relationship of the sheet resistance with CNT length is attributed to the CNT network morphology ($\propto$ number of barriers an electron must tunnel through during its percolated path). These results indicate that the CNT length can be used to tune the electrical properties of these A-CNT networks in a manner similar to tuning the bundle size in networks of unaligned single walled CNTs.[15,16] Future studies should explore the impact of CNT proximity effects and waviness on the electron transport properties of A-CNT networks via both theory (analytically) and simulation (numerically). Once CNT proximity effects can be better quantified, precise control over the electrical properties of A-CNT networks may become possible, enabling the design and fabrication of better performing sensors and actuators, optoelectronics, and energy storage devices. Such materials have already found application as mass and volume-efficient heaters for aerovehicle ice protection.[56]

[1]M. F. L. De Volder, S. H. Tawfick, R. H. Baughman, and A. J. Hart, Science **339**, 535 (2013).
[2]L. Liu, W. Ma, and Z. Zhang, Small **7**, 1504 (2011).
[3]L. Chen, C. Liu, K. Liu, C. Meng, C. Hu, J. Wang, and S. Fan, ACS Nano **5**, 1588 (2011).
[4]X. Sun, W. Wang, L. Qiu, W. Guo, Y. Yu, and H. Peng, Angew. Chem., Int. Ed. **51**, 8520 (2012).
[5]Q. Cao and J. A. Rogers, Adv. Mater. **21**, 29 (2009).
[6]J. A. Rogers, T. Someya, and Y. Huang, Science **327**, 1603 (2010).
[7]L. Hu, D. S. Hecht, and G. Grüner, Chem. Rev. **110**, 5790 (2010).
[8]C. Feng, K. Liu, J.-S. Wu, L. Liu, J.-S. Cheng, Y. Zhang, Y. Sun, Q. Li, S. Fan, and K. Jiang, Adv. Funct. Mater. **20**, 885 (2010).
[9]F. Meng, X. Zhang, G. Xu, Z. Yong, H. Chen, M. Chen, Q. Li, and Y. Zhu, ACS Appl. Mater. Interfaces **3**, 658 (2011).
[10]Z. Yang, T. Chen, R. He, G. Guan, H. Li, L. Qiu, and H. Peng, Adv. Mater. **23**, 5436 (2011).
[11]R. Allen, G. G. Fuller, and Z. Bao, ACS Appl. Mater. Interfaces **5**, 7244 (2013).
[12]Y. Yin, C. Liu, and S. Fan, J. Phys. Chem. C **116**, 26185 (2012).
[13]K. Wang, S. Luo, Y. Wu, X. He, F. Zhao, J. Wang, K. Jiang, and S. Fan, Adv. Funct. Mater. **23**, 846 (2013).
[14]H. Gwon, J. Hong, H. Kim, D.-H. Seo, S. Jeon, and K. Kang, Energy Environ. Sci. **7**, 538 (2014).
[15]D. Hecht, L. Hu, and G. Grüner, Appl. Phys. Lett. **89**, 133112 (2006).
[16]P. E. Lyons, S. De, F. Blighe, V. Nicolosi, L. F. C. Pereira, M. S. Ferreira, and J. N. Coleman, J. Appl. Phys. **104**, 044302 (2008).
[17]Q. Cao, S.-j. Han, G. S. Tulevski, Y. Zhu, D. D. Lu, and W. Haensch, Nat. Nanotechnol. **8**, 180 (2013).
[18]G. J. Brady, Y. Joo, S. Singha Roy, P. Gopalan, and M. S. Arnold, Appl. Phys. Lett. **104**, 083107 (2014).
[19]V. Derenskyi, W. Gomulya, J. M. S. Rios, M. Fritsch, N. Fröhlich, S. Jung, S. Allard, S. Z. Bisri, P. Gordiichuk, A. Herrmann, U. Scherf, and M. A. Loi, Adv. Mater. **26**, 5969 (2014).
[20]Y. Joo, G. J. Brady, M. S. Arnold, and P. Gopalan, Langmuir **30**, 3460 (2014).
[21]S. Z. Bisri, C. Piliego, J. Gao, and M. A. Loi, Adv. Mater. **26**, 1176 (2014).
[22]L. Zhang, G. Zhang, C. Liu, and S. Fan, Nano Lett. **12**, 4848 (2012).
[23]D. Wang, P. Song, C. Liu, W. Wu, and S. Fan, Nanotechnology **19**, 075609 (2008).
[24]J. Marschewski, J. B. In, D. Poulikakos, and C. P. Grigoropoulos, Carbon **68**, 308 (2014).
[25]B. L. Wardle, D. S. Saito, E. J. García, A. J. Hart, R. Guzmán de Villoria, and E. A. Verploegen, Adv. Mater. **20**, 2707 (2008).
[26]A. M. Marconnet, N. Yamamoto, M. A. Panzer, B. L. Wardle, and K. E. Goodson, ACS Nano **5**, 4818 (2011).
[27]I. Y. Stein and B. L. Wardle, Phys. Chem. Chem. Phys. **15**, 4033 (2013).
[28]A. J. Hart and A. H. Slocum, J. Phys. Chem. B **110**, 8250 (2006).
[29]I. Y. Stein and B. L. Wardle, Carbon **68**, 807 (2014).
[30]See supplementary material at http://dx.doi.org/10.1063/1.4907608 for additional morphology characterization details (Sec. S1), error

approximation for the CNT height measurement (Sec. S2), derivation of Eq. (1) in the main text (Sec. S3), and anisotropy in sheet resistance for networks comprised of short CNTs (Sec. S4).

[31]D. Handlin, I. Y. Stein, R. Guzman de Villoria, H. Cebeci, E. M. Parsons, S. Socrate, S. Scotti, and B. L. Wardle, J. Appl. Phys. **114**, 224310 (2013).

[32]M. Bedewy, E. R. Meshot, H. Guo, E. A. Verploegen, W. Lu, and A. J. Hart, J. Phys. Chem. C **113**, 20576 (2009).

[33]R. R. Mitchell, N. Yamamoto, H. Cebeci, B. L. Wardle, and C. V. Thompson, Compos. Sci. Technol. **74**, 205 (2013).

[34]I. Kazani, G. De Mey, C. Hertleer, J. Banaszczyk, A. Schwarz, G. Guxho, and L. Van Langenhove, Text. Res. J. **81**, 2117 (2011).

[35]Y. Ma, P. O. Lehtinen, A. S. Foster, and R. M. Nieminen, New J. Phys. **6**, 68 (2004).

[36]R. Singh and P. Kroll, J. Phys.: Condens. Matter **21**, 196002 (2009).

[37]G. Giambastiani, S. Cicchi, A. Giannasi, L. Luconi, A. Rossin, F. Mercuri, C. Bianchini, A. Brandi, M. Melucci, G. Ghini, P. Stagnaro, L. Conzatti, E. Passaglia, M. Zoppi, T. Montini, and P. Fornasiero, Chem. Mater. **23**, 1923 (2011).

[38]Z. He, H. Xia, X. Zhou, X. Yang, Y. Song, and T. Wang, J. Phys. D: Appl. Phys. **44**, 085001 (2011).

[39]L. G. Cançado, A. Jorio, E. H. Martins Ferreira, F. Stavale, C. A. Achete, R. B. Capaz, M. V. O. Moutinho, A. Lombardo, T. S. Kulmala, and A. C. Ferrari, Nano Lett. **11**, 3190 (2011).

[40]I. Y. Stein, N. Lachman, M. E. Devoe, and B. L. Wardle, ACS Nano **8**, 4591 (2014).

[41]D. Janas and K. K. Koziol, Nanoscale **6**, 3037 (2014).

[42]S. Tawfick, K. O'Brien, and A. J. Hart, Small **5**, 2467 (2009).

[43]S. Li, Z. Yu, C. Rutherglen, and P. J. Burke, Nano Lett. **4**, 2003 (2004).

[44]I. Balberg, N. Binenbaum, and C. H. Anderson, Phys. Rev. Lett. **51**, 1605 (1983).

[45]P. N. Nirmalraj, P. E. Lyons, S. De, J. N. Coleman, and J. J. Boland, Nano Lett. **9**, 3890 (2009).

[46]V. Skákalová, A. B. Kaiser, Y.-S. Woo, and S. Roth, Phys. Rev. B **74**, 085403 (2006).

[47]V. Skákalová, A. B. Kaiser, Z. Osváth, G. Vértesy, L. P. Biró, and S. Roth, Appl. Phys. A **90**, 597 (2008).

[48]A. B. Kaiser and V. Skákalová, Chem. Soc. Rev. **40**, 3786 (2011).

[49]M. P. Garrett, I. N. Ivanov, R. A. Gerhardt, A. A. Puretzky, and D. B. Geohegan, Appl. Phys. Lett. **97**, 163105 (2010).

[50]G. Chen, D. N. Futaba, S. Sakurai, M. Yumura, and K. Hata, Carbon **67**, 318 (2014).

[51]E. Kymakis and G. A. J. Amaratunga, J. Appl. Phys. **99**, 084302 (2006).

[52]K. Yanagi, H. Udoguchi, S. Sagitani, Y. Oshima, T. Takenobu, H. Kataura, T. Ishida, K. Matsuda, and Y. Maniwa, ACS Nano **4**, 4027 (2010).

[53]P. Sheng, E. K. Sichel, and J. I. Gittleman, Phys. Rev. Lett. **40**, 1197 (1978).

[54]P. Sheng, Phys. Rev. B **21**, 2180 (1980).

[55]M. Salvato, M. Cirillo, M. Lucci, S. Orlanducci, I. Ottaviani, M. L. Terranova, and F. Toschi, Phys. Rev. Lett. **101**, 246804 (2008).

[56]S. T. Buschhorn, S. S. Kessler, N. Lachman, J. Gavin, G. Thomas, and B. L. Wardle, *Proceedings of the 54th AIAA/ASME/ASCE/AHS/ASC Structures, Structural Dynamics, and Materials (SDM) Conference* (AIAA, 2013), paper 2013-1729.

Supplementary Information: Impact of carbon nanotube length on electron transport in aligned carbon nanotube networks

Jeonyoon Lee,[1, a)] Itai Y. Stein,[1, a)] Mackenzie E. Devoe,[2] Diana J. Lewis,[3] Noa Lachman,[3] Seth S. Kessler,[4] Samuel T. Buschhorn,[3] and Brian L. Wardle[3, b)]

[1)] *Department of Mechanical Engineering, Massachusetts Institute of Technology, 77 Massachusetts Ave, Cambridge, Massachusetts 02139, USA.*

[2)] *Department of Materials Science and Engineering, Massachusetts Institute of Technology, 77 Massachusetts Ave, Cambridge, Massachusetts 02139, USA.*

[3)] *Department of Aeronautics and Astronautics, Massachusetts Institute of Technology, 77 Massachusetts Ave, Cambridge, Massachusetts 02139, USA.*

[4)] *Metis Design Corporation, 205 Portland St, Boston, Massachusetts 02114, USA.*

[a)]J. Lee and I. Y. Stein contributed equally to this work

[b)]Electronic mail: wardle@mit.edu

S1. STRUCTURE AND MORPHOLOGY OF CARBON NANOTUBES IN ALIGNED ARRAYS

This Section contains the experimentally determined values of the CNT inner and outer diameters, from transmission electron microscopy (TEM), the origin and approximate value of the CNT intrinsic density, the experimentally determined value of the inter-CNT spacing, from scanning electron microscopy, and the equations used to extract the CNT volume fraction from the inter-CNT spacing.

A. Inner and outer diameters

The inner (D_i) and outer (D_o) diameters of the CNTs were measured from 30 TEM micrographs (JEOL 2100, 200 kV accelerating voltage) of the as-grown CNTs. To accurately estimate the average values of D_i and D_o, Gaussian functions were fit to the obtained discrete distributions (see Fig. S1 for histograms and fits) and the following values were obtained: $\approx 5.12 \pm 0.76$ nm (coefficient of determination $= 0.9715$) for D_i, and $\approx 7.78 \pm 0.85$ nm (coefficient of determination $= 0.9462$) for D_o. These values are very similar to the ones used in previous studies $(D_i \sim 5$ nm and $D_o \sim 8$ nm).[1–4] Using the average values of D_i
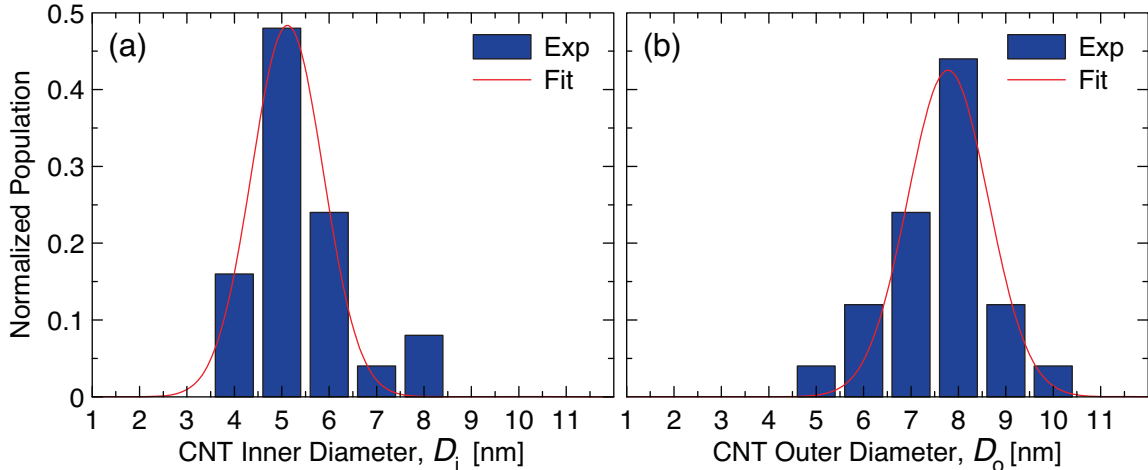

FIG. S1. (a) Histogram and fit for the CNT inner diameter (D_i) showing that $D_i \approx 5.12 \pm 0.76$ nm. (b) Histogram and fit for the CNT inner diameter (D_i) showing that $D_o \approx 7.78 \pm 0.85$ nm. These values originate from 30 transmission electron microscopy (TEM) images of the as-grown CNT arrays.

and D_o, an average number of walls of 4.9 can be evaluated, and is used in Section S1 B to evaluated the CNT intrinsic density.

B.   Intrinsic density

While most theoretical studies utilize the CNT volume fraction (V_f) as the primary measure, the majority of experimental studies only report the CNT film density, so a measure that enables the proper conversion from one to the other is necessary, and is defined as the CNT intrinsic density (ρ_cnt). As discussed in a previous study,[3] ρ_cnt is a strong function of the inner diameter and number of walls, and in order to get a proper estimate of the average ρ_cnt for an array of CNTs, the population of CNTs with respect to their number of walls needs to be properly accounted for. The previous study suggested using a discrete summation form (see Eq. S1a) to represent the probability density function of CNTs with respect to their number of walls, but a continuous integral form is more convenient, and is included below (see Eq. S1b):

$$\rho_\mathrm{cnt} = 4\rho_\mathrm{g}\ell_= \left(\sum_{k=3}^{7} \frac{p_k}{(D_\mathrm{i} + 2\ell_=(k-1))^2} \left(\sum_{j=1}^{k}(D_\mathrm{i} + 2\ell_=(j-1)) \right) \right) \tag{S1a}$$

$$\rho_\mathrm{cnt} = 4\rho_\mathrm{g}\ell_= \left(\sum_{k=3}^{7} \frac{p_k}{(D_\mathrm{i} + 2\ell_=(k-1))^2} \left(\int_0^{k}(D_\mathrm{i} + 2\ell_=(j-0.5))\,\mathrm{d}j \right) \right) \tag{S1b}$$

Where ρ_g is the theoretical density of a single graphene sheet (≈ 2.25 g/cm^3), $\ell_=$ is the inter-layer spacing value for MWCNTs (≈ 3.41 Å), D_i is the inner diameter (≈ 5.12 nm from Section S1 A), and the summation/integration limit variables j and k represent the 3 to 7 wall nature of the CNT population. To further simplify Eq. S1b, the probability distribution can be approximated with a Gaussian centered at μ with a standard deviation σ (see Fig. S2a for exemplary fits of discrete distributions centered at $\mu = 5$), enabling the first summation term to be replaced with a scaling factor $\alpha(\mu, \sigma)$ as follows:

$$\rho_\mathrm{cnt} \simeq 4\rho_\mathrm{g}\ell_=\alpha(\mu,\sigma)\frac{\mu(D_\mathrm{i} - \ell_=(1-\mu))}{(D_\mathrm{i} + 2\ell_=(\mu-1))^2} \tag{S2}$$

Where $\alpha(\mu,\sigma) \lesssim 1$ ($\to \alpha(\mu,\sigma) = 1$ corresponds to the ideal $\sigma = 0$ Delta function).

To evaluate the scaling of $\alpha(\mu, \sigma)$, Eq. S1b was studied with discrete distributions that correspond to Gaussians centered at integer values of μ ($3 \leq \mu \leq 7$) with $0.4 \lesssim \sigma \lesssim 2.0$. The resulting values of ρ_{cnt} were then compared to the ideal Delta function centered at the respective μ value (Eq. S2 with $\alpha(\mu, \sigma) = 1$), leading to the value of the scaling factor $\alpha(\mu, \sigma)$. See Fig. S2b for a plot of $\alpha(\mu, \sigma)$ as a function of σ and μ. As Fig. S2b demonstrates, $\alpha(\mu, \sigma) \gtrsim 0.98$, and since $\rho_{\mathrm{cnt}}(\mu = 4.9) = 1.602$ g/cm^3 for $\alpha(\mu, \sigma) = 1$ (ideal Delta function), $\rho_{\mathrm{cnt}} \approx 1.6$ g/cm^3 for the CNTs used in this study regardless of the distribution of the CNTs with respect to their number of walls (assuming the form remains Gaussian in nature) .
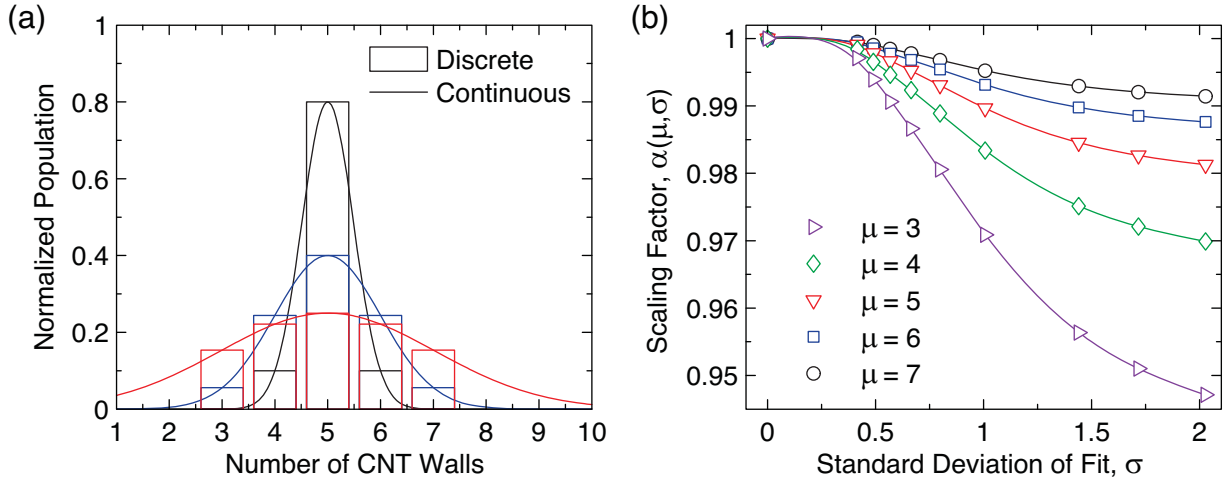

FIG. S2. (a) Exemplary Gaussian fits of discrete distributions centered at 5 ($\rightarrow \mu = 5$) with standard deviations (σ) of ~ 0.5, 1, and 2. (b) Plot of scaling factor, $\alpha(\mu, \sigma)$, of the average CNT intrinsic density as a function of μ and σ. According to the empirical scaling relationship, $\alpha(\mu, \sigma) \gtrsim 0.98$ for the CNTs used in this study ($\mu \approx 4.9$ and $\sigma \sim 1$), meaning that the average CNT intrinsic density ~ 1.6 g/cm^3.

C. Packing morphology and volume fraction

A previous study[2] included a detailed discussion of the scaling relationship between the average inter-CNT spacing (Γ), the CNT volume fraction (V_f), the CNT outer diameter (D_o), and the notional two dimensional coordination number (N) of an idealized aligned CNT system. The functional forms of this scaling relationship are included in Eq. S3 below:[2]

$$\Gamma = D_\text{o} \left((11.77(N)^{-3.042} + 0.9496) \sqrt{\frac{\sqrt{3}\pi}{6V_\text{f}}} - 1 \right) \tag{S3a}$$

$$N = 2.511(V_\text{f}) + 3.932 \tag{S3b}$$

Using the isosceles angle (θ) of the constitutive triangles at each N, the minimum (Γ_min) and maximum (Γ_max) inter-CNT spacings were previously separated from Γ (Eq. S3a), yielding the following:[4]

$$\theta = \pi \left(\frac{1}{2} - \frac{1}{N} \right) \tag{S4a}$$

$$\Gamma_\text{max} = 4\cos(\theta) \left(\frac{\Gamma}{1 + 2\cos(\theta)} \right) \tag{S4b}$$

$$\Gamma_\text{min} = 2 \left(\frac{\Gamma}{1 + 2\cos(\theta)} \right) \tag{S4c}$$

To evaluate the V_f of the CNTs in the as-grown arrays, the average inter-CNT spacing must first be evaluated experimentally, and is defined as Γ^exp. Γ^exp was evaluated from 15 SEM micrographs (JEOL 6700, 6.0 mm working distance) by first adjusting their contrast to have 0.5% saturated pixels, and then reducing noise by applying a median filter. All processing was done in ImageJ. Γ^exp was estimated from these images by counting the number of in-focus (bright) CNT, and dividing the width of the picture by that number. The counting was done by taking a line plot across two places on the image, where peaks with a brightness greater than 150 (on a $0 - 255$ scale) were counted as a single CNT. A histogram of Γ^exp, along with a gaussian fit (coefficient of determination $= 0.9913$), can be found in Fig. S3a. The gaussian fit indicates that $\Gamma^\text{exp} \approx 58.6 \pm 10.6$ nm.

Using Eq. S3 and Eq. S4, Γ^{exp} can be used to approximate V_{f} for $D_{\text{o}} \approx 7.78$ nm (from Section S1 A), where the mean of Γ^{exp} is approximately equal to Γ ($\rightarrow \Gamma \approx 58.6$ nm), and the standard deviations of Γ^{exp} are used to define Γ_{min} ($\rightarrow \Gamma_{\text{min}} \approx 48.0$ nm) and Γ_{max} ($\rightarrow \Gamma_{\text{min}} \approx 69.2$ nm). The resulting estimates indicate that 1.567 vol. % $\lesssim V_{\text{f}} \lesssim 1.604$ vol. %, meaning that $V_{\text{f}} \sim 1.6$ vol. % for the as-grown CNT arrays used in this study. See Fig. S3b for a comparison of the V_{f} estimate, Γ, Γ_{min} and Γ_{max}.
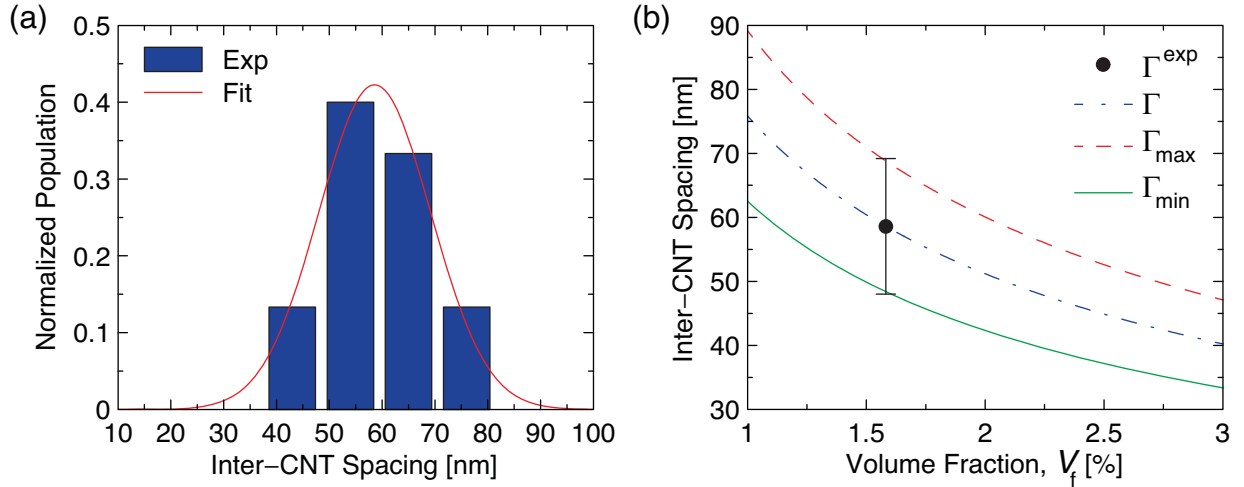

FIG. S3. (a) Histogram and fit for the experimentally determined inter-CNT spacing (Γ) showing that $\Gamma^{\text{exp}} \approx 58.6 \pm 10.6$ nm. These values originate from 15 scanning electron microscopy (SEM) micrographs of the cross-sectional morphology of the as-grown CNT arrays. (b) Comparison of Γ^{exp} to Γ (Eq. S3a), Γ_{min} (Eq. S4b), Γ_{max} (Eq. S4c) illustrating that $V_{\text{f}} \approx 1.6$ vol. % CNTs in the as-grown CNT arrays used to synthesize the aligned CNT films.

S2. ERROR OF CARBON NANOTUBE LENGTH MEASUREMENT

As discussed in the main text, the two main sources of error for this measurement are the CNT waviness, and the entangled growth initiation region. Since the growth initiation region is on the order of ~ 0.1 μm -1 μm thick, error originating from the CNT waviness is the focus of this calculation. The error induced by waviness can be estimated by first assuming a simple sinusoidal shape for the wavy CNTs (see Fig. S4 for illustration), and varying the waviness ratio (w), which is the ratio of the amplitude (a) to wavelength (λ) of the sinusoid. The length of CNTs accounting for waviness (L) can then be compared to that of the height of the aligned CNT forest (H) as follows (see Fig. S4 for the error as a function of w):

$$\frac{L}{H} = 2 \int_{0}^{\frac{1}{2}} \sqrt{\left(1 + \left(2\pi w \cos\left(2\pi x\right)\right)^2\right)} \, \mathrm{d}x \tag{S5}$$

As Fig. S4 illustrates, $L \sim 1.5H$ for the w of the as-grown CNTs ($w \sim 0.25$).
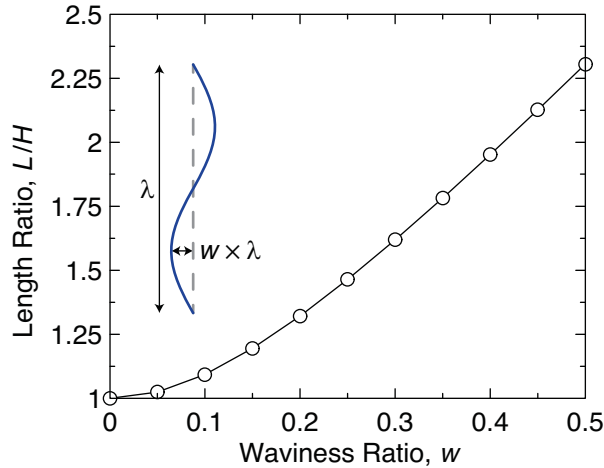

FIG. S4. Illustration of the waviness approximation where the waviness ratio (w) is defined using the ratio of the amplitude of the sinusoid and the wavelength (λ), and a Plot of the ratio of the true CNT length (L) and the height of the CNT forest (H) as a function of w evaluated using Eq. S5. Neglecting the waviness of the CNTs can lead to errors of $\gtrsim 100\%$ when using H as an approximation of L.

S3. SHEET RESISTANCE AS A FUNCTION OF ORIENTATION

The values of the components of the resistivity tensor change depending on the orientation of the CNTs. Assuming that the longitudinal, transverse, and through-thickness directions of the aligned CNT film correspond to eigenvectors, the resistivity tensor $\boldsymbol{\rho}$ can be described by its eigenvalues: $\hat{\rho}_1$, $\hat{\rho}_2$, and $\hat{\rho}_3$; and the rotation matrix A with corresponding Euler angles in each axis. If the aligned CNT film is rotated normal to the film thickness with an angle θ, the new resistivity tensor can be defined as:

$$\boldsymbol{\rho} = A^T \hat{\boldsymbol{\rho}} A \tag{S6a}$$

$$\hat{\boldsymbol{\rho}} = \begin{bmatrix} \hat{\rho}_1 & 0 & 0 \\ 0 & \hat{\rho}_2 & 0 \\ 0 & 0 & \hat{\rho}_3 \end{bmatrix} \tag{S6b}$$

$$A = \begin{bmatrix} \cos(\theta) & \sin(\theta) & 0 \\ -\sin(\theta) & \cos(\theta) & 0 \\ 0 & 0 & 1 \end{bmatrix} \tag{S6c}$$

The resistivity of the CNT film as a function of angle θ, $\rho(\theta)$, can then be described using $\boldsymbol{\rho}(1,1)$ (the first term of $\boldsymbol{\rho}$ in $\boldsymbol{\rho}(m,n)$ notation, where m designates the row and n the column), and $\hat{\rho}_1$ (defined as $\rho(\theta = 0°)$ in the main text) and $\hat{\rho}_2$ (defined as $\rho(\theta = 90°)$ in the main text):

$$\begin{aligned} \rho(\theta) = \rho(1,1) &= \hat{\rho}_1 \cos^2 \theta + \hat{\rho}_2 \sin^2 \theta \\ &= \rho(\theta = 0°) \cos^2 \theta + \rho(\theta = 90°) \sin^2 \theta \end{aligned} \tag{S7}$$

Since sheet resistance (R) can be calculated by dividing $\rho(\theta)$ by the film thickness, R as a function of angle θ can be modeled as follows:

$$R(\theta) = R(\theta = 0°) \cos^2 \theta + R(\theta = 90°) \sin^2 \theta \tag{S8}$$

S4. ANISOTROPY IN SHEET RESISTANCE FOR NETWORKS COMPRISED OF SHORT CARBON NANOTUBES

As discussed in the main text (see Fig. 2b), buckling and/or squashing strongly affects the electrical properties of the A-CNT networks comprised of CNTs with $L < 150 \, \mu$m, and leads to an anisotropy $(R(\theta = 90°)/R(\theta = 0°))$ of $\sim 19\%$, which is much lower than the value observed for A-CNT networks comprised of longer $(L > 150 \, \mu$m) CNTs ($\rightarrow \sim 44\%$). See Fig. S5 for a plot comparing $R(\theta)$ for A-CNT networks comprised of CNTs with $L < 150 \, \mu$m and $L > 150 \, \mu$m.
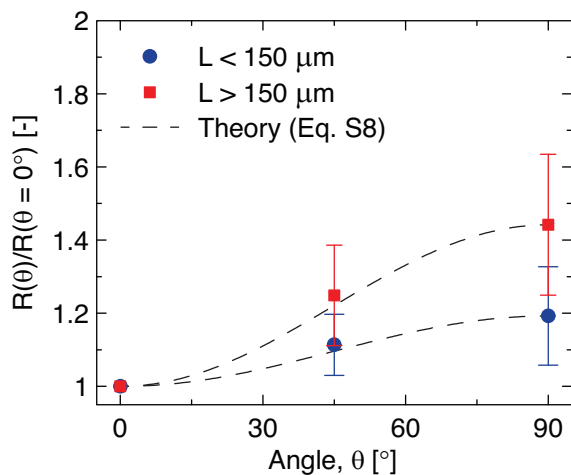

FIG. S5. Sheet resistance (R) of A-CNT networks as a function of orientation (θ) for $L < 150 \, \mu$m and $L > 150 \, \mu$m demonstrating that the anisotropy of A-CNT networks comprised of longer $(L > 150 \, \mu$m) CNTs is higher $(R(\theta = 90°)/R(\theta = 0°) \sim 1.44 \pm 0.19)$ than the anisotropy of A-CNT networks comprised of CNTs with $L < 150 \, \mu$m $(R(\theta = 90°)/R(\theta = 0°) \sim 1.19 \pm 0.13)$.

REFERENCES

[1] A. J. Hart and A. H. Slocum, J. Phys. Chem. B **110**, 8250 (2006).

[2] I. Y. Stein and B. L. Wardle, Phys. Chem. Chem. Phys. **15**, 4033 (2013).

[3] I. Y. Stein and B. L. Wardle, Carbon **68**, 807 (2014).

[4] I. Y. Stein, N. Lachman, M. E. Devoe, and B. L. Wardle, ACS Nano **8**, 4591 (2014).